Available online at www.sciencedirect.com
ScienceDirect
Journal of Photochemistry and Photobiology A: Chemistry 190 (2007) 190–199
Journal of Photochemistry and Photobiology A:Chemistry
www.elsevier.com/locate/jphotochem

A model Hamiltonian to simulate the complex photochemistry of benzene

G.A. Worth *

School of Chemistry, University of Birmingham, Birmingham B15 2TT, UK

Available online 21 January 2007

Abstract

The photochemistry and photophysics of benzene is a classic example of the richness of competing pathways available to a molecule after photo-excitation. Computer simulations are one way to provide a molecular picture for the dynamics behind the experimental observables. In this paper a first step is made towards quantum dynamics simulations of benzene by setting up a vibronic coupling model Hamiltonian to provide the potential energy functions that drive the nuclear motion. Seven coupled states and all vibrational modes are included and the parameters for the model obtained by fitting to points provided by quantum chemistry calculations. The model is shown to be a good fit of the adiabatic surfaces. A full vibronic analysis is made revealing the complexity of the features of this manifold of states. Low-level CASSCF calculations have been used here, and future calculations using higher level methods will build on this work to make the model suitable for the correct description of benzene.

Keywords: Benzene photochemistry; Wavepacket dynamics; Vibronic coupling; Conical intersections

1. Introduction

The photophysics and photochemistry of benzene has been studied extensively, both theoretically [1–6] and experimentally [7–13]. Despite the simplicity of the molecule, with its perfectly regular and symmetrical structure, it provides a classic example of the richness of photochemistry, with a number of possible competing outcomes after photo-excitation. Much of this has been well characterised, but questions still remain.

The most powerful way to elucidate the dynamical behaviour behind observables is to use computer simulations. Wavepacket dynamics give particularly easy to visualise results, with the system described by a wavepacket that evolves in time after being initially prepared in a way that can be related directly to a particular experiment [14–17]. This paper represents the first step towards such a study of the photochemistry of benzene, namely setting up potential energy functions, at this stage qualitative and incomplete, to describe the dynamics of benzene in the manifold of states involved.

The absorption spectrum of benzene shows three bands between 4.5 and 8 eV [9]. These are the $\tilde{A}^1B_{2u}$, $\tilde{B}^1B_{1u}$, and $\tilde{C}^1E_{1u}$ states. The $\tilde{A}$ and $\tilde{B}$ bands are forbidden, while $\tilde{C}$ is an intense, fairly structureless band. Describing the ground-state configuration of benzene by the valence- π orbitals formed by the six carbon $2p_z$ orbitals gives $a_{2u}^2e_{1g}^4e_{2u}^0b_{2g}^0$ with six electrons in the lowest three orbitals. The $\pi \rightarrow \pi*$ transition $a_{2u}^2e_{1g}^3e_{2u}^1b_{bg}^0$ leads to four states, which are those seen in the spectrum.

Photophysical data shows that fluorescence from $\tilde{A}$ vanishes if the molecule is excited 3000 cm^{-1} above the band origin [10]. This process, which is termed "channel 3", is due to a conical intersection between $\tilde{A}$ and the $\tilde{X}^1A_{1g}$ ground-state which becomes accessible at this energy. Theoretical studies by Robb et al. showed that this is due to a barrier between the Franck–Condon point and the conical intersection which is surmounted at this energy [2]. Recent studies have looked at how channel 3 is accessed after exciting specific modes [11].

Conical intersections are known to play a crucial role in a wide variety of photochemical processes [18–21]. These are a special topology of the adiabatic potential energy surfaces of a molecule where in a two-dimensional space of nuclear coordinates two surfaces meet at the point of a double cone. Due to coupling between the electronic and nuclear motion in these regions of the potential surfaces, conical intersections provide pathways for efficient internal conversion as the system can pass from one electronic state to another effectively instantaneously

* Corresponding author. Tel.: +44 121 414 3782.
E-mail address: G.A.Worth@bham.ac.uk.

1010-6030/$ – see front matter © 2007 Elsevier B.V. All rights reserved.
doi:10.1016/j.jphotochem.2007.01.020

in a radiationless manner. Much recent work has been made to study the interesting properties of these intersections and the effect on molecular dynamics as a molecule passes through one [20–22].

The photochemical products of benzene are fulvene, benzvalene and Dewar benzene [7,8]. These are formed in different amounts according to the excitation wavelength used. Exciting into the $\tilde{A}$ band at 254 nm the quantum yields are 0.01:0.01:0.00, respectively. Raising the energy increases the yields slightly. Exciting into the $\tilde{B}$ band at 165 nm gives very different yields of 0.05:0.02:0.01. It has demonstrated that the $\tilde{X}/\tilde{A}$ conical intersection plays an important role in this as it leads directly to prefulvene, the precursor for the transformations [2]. Relaxation from the $\tilde{B}$ state is found to occur on a 40 fs timescale, with no evidence of significant population of the $\tilde{A}$ state during this process [23].

Computer simulations require potential energy functions to drive the nuclear motion. The calculation of a function is often a long and tedious process. Typically, quantum chemistry calculations are made at a range of geometries and a suitable function fit to these energies. This function can then be improved by higher level calculations and/or experimental information until calculated molecular properties match experimental observables. Often many thousands of points need to be calculated, with the number rising exponentially with the number of degrees of freedom.

In this paper a potential operator matrix suitable for benzene photochemistry is set up using simple functions parameterised by fitting to the adiabatic potential surfaces. This function is the vibronic coupling model Hamiltonian [24], which has been shown to be able to describe the dynamics of a number of systems in which conical intersections dominate. One of these is the benzene radical cation formed during the photo-ionisation of benzene while measuring the photo-electron spectrum [25]. The simplicity of the model allows a natural description of the photo-initiated dynamics in terms of the excitation of normal mode vibrations and couplings between diabatic states which can be correlated to electronic configurations, i.e. distinct chemical entities. Together with the powerful MCTDH wavepacket dynamics method [17,26] the vibronic coupling model Hamiltonian has been able to give insight into the non-adiabatic dynamics of a number of systems [21,27].

To provide data points representing the adiabatic potential surfaces over a wide range of geometries, CASSCF calculations have been used. While it is necessary to include dynamic correlation for an accurate description of benzene (see Section 2.3), these calculations at least provide a reasonable model in the sense that all the desired states are included. The important result is that the fitting procedure used here provides a vibronic coupling model able to follow and describe the complicated behaviour of the seven coupled adiabatic surfaces calculated at this level. The symmetry analysis made of the couplings is also independent of the actual surfaces. Work is presently underway to take the model obtained here and use high-level methods to re-parameterise the model so that it is able to describe the observed photochemistry of benzene.

Table 1
Energies of lowest six singlet excited states of benzene

State	SA-CAS(6,6)	CASPT2[a]	Experimental[b]
$\tilde{A}^1B_{2u}$	4.895	4.84	4.90
$\tilde{B}^1B_{1u}$	8.166	6.30	6.20
$\tilde{C}^1E_{1u}$	9.542	7.03	6.94
$\tilde{D}^1E_{2g}$	8.110	7.90	7.8

The SA-CAS(6,6) used a 6-31G* basis set and are averaged over all six states plus the ground-state.
[a] Ref. [6].
[b] $\tilde{A}$–$\tilde{C}$[12], $\tilde{D}$ [13].

2. Theory

2.1. The benzene vibronic coupling model Hamiltonian

In the energy region in which we are interested, spanning less than 3 eV, benzene has six excited singlet states. At the Franck–Condon point – the ground-state minimum energy geometry – benzene has D_{6h} symmetry. In addition to the ground-state $\tilde{X}^1A_{1g}$, the excited states are $\tilde{A}^1B_{2u}$, $\tilde{B}^1B_{1u}$, $\tilde{C}^1E_{1u}$, and $\tilde{D}^1E_{2g}$. The energies of these states are given in Table 1.

The model Hamiltonian is a matrix representation in a diabatic electronic basis [24]. For benzene, a 7×7 matrix is required to represent the states (six excited states plus the ground-state). The on-diagonal matrix elements are the diabatic potential surfaces and the off-diagonal elements the state couplings. These functions are expanded as Taylor series around the Franck–Condon point using dimensionless (mass-frequency scaled) normal mode coordinates. The Franck–Condon point, $\mathbf{Q} = 0$, is denoted $\mathbf{Q}_0$. The symmetries and frequencies of the

Table 2
Frequencies of benzene at the D_{6h} minimum energy geometry compared to experimental results

Mode[a]	Symmetry	CAS(6,6)	Experimental[b]
1 (2)	$1a_{1g}$	0.1292	0.1231
2 (1)	$2a_{1g}$	0.4198	0.3811
3 (3)	$1a_{2g}$	0.1861	0.1674
4 (8)	$1b_{2g}$	0.0898	0.0877
5 (7)	$2b_{2g}$	0.1286	0.1227
6 (18)	$1e_{2g}$	0.0886	0.0754
7 (15)	$4e_{2g}$	0.4160	0.3790
8 (16)	$3e_{2g}$	0.2157	0.1985
9 (17)	$2e_{2g}$	0.1582	0.1460
10 (11)	$1e_{1g}$	0.1086	0.1050
11 (4)	$1a_{2u}$	0.0811	0.0834
12 (6)	$1b_{1u}$	0.1363	0.1252
13 (5)	$2b_{1u}$	0.4148	0.3790
14 (9)	$2b_{2u}$	0.1662	0.1623
15 (10)	$1b_{2u}$	0.1470	0.1423
16 (20)	$1e_{2u}$	0.0535	0.0493
17 (19)	$2e_{2u}$	0.1231	0.1199
18 (14)	$1e_{1u}$	0.1382	0.1287
19 (13)	$2e_{1u}$	0.2021	0.1840
20 (12)	$3e_{1u}$	0.4183	0.3799

All values in eV. The calculations were at the CAS(6,6)/6-31G* level.
[a] Wilson [33] (Herzberg [34]) numbering.
[b] Ref. [35].

normal mode coordinates of benzene are listed in Table 2. Two common numbering systems are used for these: the Wilson and Herzberg schemes. The former will be used throughout this paper, and the Herzberg numbering is included in brackets as a comparison in the table. The components of the doubly degenerate modes are labelled a and b, e.g. $\nu_{16a}(1e_{2u})$ is one component of the low frequency boat/twist pair, in fact it is the boat mode. The most important modes for the discussion of the model are shown in Fig. 1.

It is useful to write the Hamiltonian as a sum of a zero-order Hamiltonian $H^{(0)}$, and a set of "diabatic coupling" matrices $\mathbf{W}^{(k)}$:

$$\mathbf{H} = H^{(0)}\mathbf{1} + \mathbf{W}^{(0)} + \mathbf{W}^{(1)} + \cdots \tag{1}$$

The zero-order Hamiltonian is simply the ground-state Hamiltonian in the harmonic approximation:

$$H^{(0)} = \sum_{\alpha} \frac{\omega_\alpha}{2}\left(\frac{\partial^2}{\partial Q_\alpha^2} + Q_\alpha^2\right) \tag{2}$$

with vibrational frequencies ω_α. The zero-order coupling matrix is diagonal, with the energies of the electronic states at $\mathbf{Q}_0$. As the diabatic electronic states are set equal to the adiabatic states at this point, these energies are the adiabatic state energies:

$$W_{ii}^{(0)} = E_i \tag{3}$$

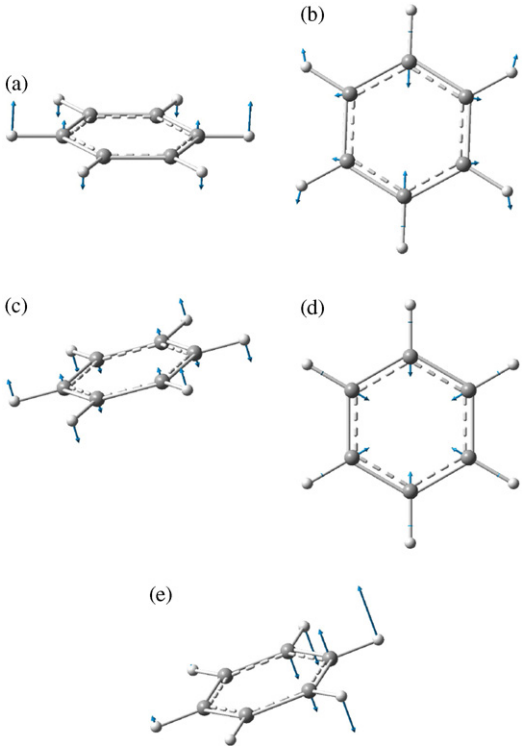

Fig. 1. The normal modes of benzene important for a description of its photochemistry: (a) $\nu_{16a}(1e_{2u})$, the boat mode; (b) $\nu_{6a}(1e_{2g})$, a quinoid mode; (c) $\nu_4(1b_{2g})$, the chair mode; (d) $\nu_1(1a_{1g})$, the carbon breathing mode; (e) the combined $\nu_{16a} + \nu_4$ mode.

The first-order coupling matrix contains linear terms in the Taylor expansions

$$W_{ii}^{(1)} = \sum_{\alpha} \kappa_\alpha^{(i)} Q_\alpha \tag{4}$$

$$W_{ij}^{(1)} = \sum_{\alpha} \lambda_\alpha^{(i,j)} Q_\alpha, \quad i \neq j \tag{5}$$

The on-diagonal expansion coefficients, $\kappa^{(i)}$, are related to the derivative of the adiabatic potential with respect to the coordinates, while the off-diagonal coefficients, $\lambda^{(i,j)}$, is the non-adiabatic coupling between the states:

$$\kappa_\alpha^{(i)} = \left\langle \Phi_i \left| \frac{\partial H_{\mathrm{el}}}{\partial Q_\alpha} \right| \Phi_i \right\rangle \tag{6}$$

$$\lambda_\alpha^{(i,j)} = \left\langle \Phi_i \left| \frac{\partial H_{\mathrm{el}}}{\partial Q_\alpha} \right| \Phi_j \right\rangle \tag{7}$$

where H_{el} is the usual electronic Hamiltonian at a particular nuclear geometry and Φ_i its eigenfunctions, the adiabatic electronic wavefunctions at this point. The matrix elements are evaluated at $\mathbf{Q}_0$.

Further coupling matrices follow this pattern. For example the second-order matrix has elements:

$$W_{ii}^{(2)} = \frac{1}{2}\sum_{\alpha,\beta} \gamma_{\alpha\beta}^{(i)} Q_\alpha Q_\beta \tag{8}$$

$$W_{ij}^{(2)} = \frac{1}{2}\sum_{\alpha,\beta} \mu_{\alpha\beta}^{(i,j)} Q_\alpha Q_\beta, \quad i \neq j \tag{9}$$

where $\gamma_{\alpha\beta}^{(i)}$ and $\mu_{\alpha\beta}^{(i,j)}$ are the second derivatives of the Hamiltonian matrix elements in the adiabatic electronic basis at $\mathbf{Q}_0$:

$$\gamma_{\alpha\beta}^{(i)} = \left\langle \Phi_i \left| \frac{\partial^2 H_{\mathrm{el}}}{\partial Q_\alpha \partial Q_\beta} \right| \Phi_i \right\rangle \tag{10}$$

$$\mu_{\alpha\beta}^{(i,j)} = \left\langle \Phi_i \left| \frac{\partial^2 H_{\mathrm{el}}}{\partial Q_\alpha \partial Q_\beta} \right| \Phi_j \right\rangle \tag{11}$$

An important feature of the model is that if symmetry is present many of the expansion coefficients must be zero as an integral is non-zero only if the integrand is a totally symmetric function. Thus the linear coefficients are zero unless the product of symmetries of the electronic states and the normal mode in the integrand is symmetric. For D_{6h} this can be written:

$$\Gamma_i \otimes \Gamma_j \otimes \Gamma_\alpha \supset A_{1g} \tag{12}$$

where Γ_i, Γ_j are the symmetries of the electronic states and Γ_α the symmetry of the coordinate. From this it can be deduced that on-diagonal coefficients, $\kappa^{(i)}$, are non-zero for a_{1g} modes. Unless the state is degenerate, all other coefficients are zero. Off-diagonal coefficients depend on the symmetries of the states. For example $\lambda^{(2,3)}$ connects the $\tilde{A}^1B_{2u}$ and $\tilde{B}^1B_{1u}$ states, and as $B_{2u} \otimes B_{1u} = A_{2g}$, non-zero linear coefficients are only found for modes with a_{2g} symmetry.

Degenerate states provide a complication. In the states of interest there are E_{1u} and E_{2g} states present. In D_{6h}, $E_{1u} \otimes$

$E_{1u} = A_{1g} + E_{2g}$. Thus modes with E_{2g} symmetry can have linear terms on the diagonal as well as the off-diagonal. This is the $E \otimes e$ Jahn–Teller effect in which the degeneracy of a doubly degenerate state is lifted by a doubly degenerate vibration leading to a lowering of symmetry. One of the pair of modes is on-diagonal and one off-diagonal. But which? The easiest way to answer this question is to look at the symmetries of the states and modes using the D_{2h} point group. This is the largest Abelian point-group, i.e. without degenerate irreps, that is a subset of D_{6h}. If a coefficient must be zero at D_{2h} it must also be zero at D_{6h}. The lower symmetry however means that potentially non-zero coefficients at D_{2h} may be zero at the higher symmetry. At D_{2h} an e_{2g} mode goes to $a_g + b_{3g}$. The component that goes to a_g thus enters on the diagonal of the coupling matrix, while the b_{3g} component goes on the off-diagonal.

The scheme of symmetries for modes with non-zero linear coupling constants are tabulated in Table 3. This can be used to set up the linear terms in the model Hamiltonian. For example, coupling between $\tilde{X}A_{1g}$ and $\tilde{A}B_{2u}$ is non-zero for modes with b_{2u} symmetry and

$$W^{(1)}_{1,2} = \sum_{\alpha=14,15} \lambda^{(1,2)}_{\alpha} Q_{\alpha} \tag{13}$$

The definitions for how the components of the doubly degenerate states transform at D_{2h} are also given in the table. It is taken that the a component translates as x and the b as y.

In the $E \otimes e$ Jahn–Teller interaction, the linear coupling matrices have 2×2 blocks for the states $i, i+1$ with $i = 4, 6$:

$$W^{(1)}_{\{i,i+1\}} = \sum_{\alpha=6-9} \begin{pmatrix} \kappa^{(i)}_{\alpha} Q_{\alpha,x} & \lambda^{(i,i+1)}_{\alpha} Q_{\alpha,y} \\ \lambda^{(i,i+1)}_{\alpha} Q_{\alpha,y} & \kappa^{(i+1)}_{\alpha} Q_{\alpha,x} \end{pmatrix},$$

$$\kappa^{(i)}_{\alpha} = -\kappa^{(i+1)}_{\alpha} = \lambda^{(i,i+1)}_{\alpha} \tag{14}$$

as modes 6–9 have the symmetry e_{2g}. The constraint on the coefficients in Eq. (14) is a consequence of the symmetry of this interaction.

Pseudo-Jahn–Teller interactions can also be present. These occur when a doubly degenerate state is coupled to a singly degenerate state through a doubly degenerate mode. The two components of the mode couple to different components of the state as shown in Table 3.

Table 3
Linear coupling scheme for the lowest singlet electronic states of benzene

	A_{1g}	B_{2u}	B_{1u}	$E_{1u,x}$ [a]	$E_{1u,y}$ [b]	$E_{2g,x}$ [c]	$E_{2g,y}$ [d]
$\tilde{X}^1A_{1g}$	a_{1g}	b_{2u}	b_{1u}	$e_{1u,x}$	$e_{1u,y}$	$e_{2g,x}$	$e_{2g,y}$
$\tilde{A}^1B_{2u}$		a_{1g}	a_{2g}	$e_{2g,y}$	$e_{2g,x}$	$e_{1u,y}$	$e_{1u,x}$
$\tilde{B}^1B_{1u}$			a_{1g}	$e_{2g,x}$	$e_{2g,y}$	$e_{1u,x}$	$e_{1u,y}$
$\tilde{C}^1E_{1u,x}$				a_{1g}, $e_{2g,x}$	$e_{2g,y}$	b_{1u}, $e_{1u,x}$	b_{2u}, $e_{1u,y}$
$\tilde{C}^1E_{1u,y}$					a_{1g}, $e_{2g,x}$	b_{2u}, $e_{1u,y}$	b_{1u}, $e_{1u,x}$
$\tilde{D}^1E_{2g,x}$						a_{1g}, $e_{2g,x}$	$e_{2g,y}$
$\tilde{D}^1E_{2g,y}$							a_{1g}, $e_{2g,x}$

Vibrational modes with the symmetry shown in the table have non-zero linear coupling parameters for the states indicated. The reduction of symmetry for the components of the doubly degenerate modes on going from D_{6h} to D_{2h} is also given.

[a] At D_{2h}, $E_{1u,x} \rightarrow B_{1u}$.
[b] At D_{2h}, $E_{1u,y} \rightarrow B_{2u}$.
[c] At D_{2h}, $E_{2g,x} \rightarrow A_g$.
[d] At D_{2h}, $E_{2g,y} \rightarrow B_{3g}$.

The second-order (quadratic and bilinear-linear) terms can be analysed in the same way. The rule is that the expansion coefficient for a bilinear-linear term is

$$\Gamma_i \otimes \Gamma_j \otimes \Gamma_{\alpha} \otimes \Gamma_{\beta} \supset A_{1g} \tag{15}$$

Thus all modes can have on-diagonal non-zero quadratic terms and on-diagonal bilinear-linear are present involving different modes with the same symmetry. Off-diagonal terms again depend on the symmetry of the states involved: the product of the symmetry of the modes must be the same as the symmetry of the active linear modes listed in Table 3.

A few modes had fourth-order terms added to the diabatic potential. This has been found previously to be important in cases where the diabatic potential becomes less harmonic at large deviations [28]. For these modes the diabatic surfaces are thus described for state i by

$$V^{(i)}_{\alpha} = E_i + \frac{\omega_{\alpha}}{2} Q^2_{\alpha} + \frac{\gamma^{(i)}_{\alpha\alpha}}{2} Q^2_{\alpha} + \frac{\epsilon^{(i)}_{\alpha}}{24} Q^4_{\alpha} \tag{16}$$

2.2. Fitting the model parameters

The adiabatic potential energy surfaces are the eigenvalues of the diabatic Hamiltonian matrix equation (1). A model Hamiltonian using a particular set of parameters, which are the expansion coefficients discussed above, can thus provide the adiabatic potential energy surfaces by diagonalising the matrix at a particular value of $\mathbf{Q}$. As a result, the parameters can be obtained by a fit of the model to adiabatic potential energy surfaces obtained from quantum chemistry calculations.

The fit was carried out as follows using the VCHAM program. This program, which helps to automate the procedure, is distributed with the MCTDH quantum dynamics package [29]. It has been used previously to provide model Hamiltonians in a number of systems [28,30,31].

The starting point is the ground-state minimum energy D_{6h} structure, $\mathbf{Q}_0$. The coordinates for the model Hamiltonian are obtained from the dimensionless (mass-frequency scaled) normal modes at this point. Using the quantum chemistry calculations detailed below, the seven surfaces were calculated with a spacing of $\Delta Q = 1.0$ at 11 points along each normal mode (five either side of $\mathbf{Q}_0$). A database was then set up containing this information. The parameters were then obtained by a least-squares fit using a simple conjugate gradient optimisation routine with the mean-square difference between the ab initio and model adiabatic energies at all the points as a penalty function.

It was subsequently found that more points were needed along the low frequency $\nu_{16}(1e_{2u})$ modes. A further eight points with a spacing of $\Delta Q = 1.0$ were calculated along these modes (four points either side of $\mathbf{Q}_0$ starting at $Q_{16} = \pm 6$) and added to the database before finalising the fit along these coordinates. A further seven points either side of $\mathbf{Q}_0$ with a spacing of $\Delta Q = 2.0$ were also calculated along the diagonals between $\nu_4(1b_{2g})$ and $\nu_{16a}(1e_{2u,x})$, and $\nu_4(1b_{2g})$ and $\nu_{16b}(1e_{2u,y})$.

Due to the dependencies between the parameters of different order the fit is performed in stages, first optimising the linear parameters before including the higher-order ones. The linear Hamiltonian has a total of 93 parameters that need to be evaluated. This demonstrates the power of using the symmetry. There are 796 linear expansion coefficients, but most are zero. The final model, which includes all the on-diagonal quadratic terms, as well as quartic terms for some modes and critical off-diagonal bilinear terms, has 2132 expansion coefficients, of which 243 are non-zero parameters that need to be obtained from the fit.

2.3. Quantum chemistry calculations

Calculations of Bernhardsson et al. [4] show that the energetics of the benzene excited states can be accurately represented using CASPT2 calculations and a large ANO basis set. A comparison of vertical excitation energies calculated at this level with experimental values is given in Table 1.

For the calculations here, a much cheaper method was used to allow a large number of calculations to be performed quickly. The idea is to provide a model at a qualitatively reasonable level that will identify the important modes and configurations. Later, high-level calculations can then focus on these regions. SA-CAS(6,6)/6-31G* was selected with the six electrons of the active space distributed in the 6-π orbitals formed by the carbon 2p orbitals. State averaging was used over the seven states of interest to provide a balanced treatment and to provide all the energies in a single calculation. The Gaussian03 program was used for all calculations [32].

The CAS(6,6) active space is that used in the CASPT2 calculations of Bernhardsson et al. [4], and is able to describe the $\tilde{A}$ and $\tilde{D}$ states very well. It has been shown, however, that it is not adequate for an accurate description of the $\tilde{B}$ and $\tilde{C}$ states due to their ionic character and mixing of Rydberg orbitals [3,6]. This will be addressed by later calculations and here we will assume that this level of calculation will at least qualitatively describe the topology of the potential energy surfaces.

The excitation energies at this level of theory are given in Table 1. All states are far too high in energy, especially the $\tilde{B}^1B_{1u}$ and $\tilde{C}^1E_{1u}$ which are approximately 2.5 eV too high. Calculations using larger basis sets and including diffuse functions make little improvement, and comparison with the CASPT2 results indicates that this error is due to a lack of dynamic correlation. Again it must be iterated that for the present purposes it is enough if the method is qualitatively correct, and the adiabatic surfaces have reasonable topologies.

3. Results

The CAS(6,6)/6-31G* frequencies, which provide the zero-order diabatic surfaces, are listed in Table 2. They are in reasonable agreement with the experimental values, with the modes in the correct order. As is usual in methods lacking dynamic correlation, the four highest frequency modes are too high. The error here is about 0.035 eV (280 cm^{-1}). Lower modes have errors of the order of 0.01 eV (90 cm^{-1}).

The $\tilde{A}$, $\tilde{B}$ and $\tilde{C}$ states can be described by predominantly HOMO–LUMO transitions, i.e. the states are formed primarily by wavefunctions with configurations $a_{2u}^2e_{1g}^3e_{2u}^1b_{2g}^0$. The wavefunction for the $\tilde{D}$ state is more complicated. Both components are dominated by four configurations: two HOMO–LUMO double excitations with configuration $a_{2u}^2e_{1g}^2e_{2u}^2b_{2g}^0$, a (HOMO −1)–LUMO configuration $a_{2u}^1e_{1g}^4e_{2u}^1b_{2g}^0$ and a HOMO–(LUMO+1) configuration $a_{2u}^2e_{1g}^3e_{2u}^0b_{2g}^1$.

The parameters obtained from the fitting procedure are listed in Tables 4–8 and cuts through the most important modes are shown in Figs. 2 and 3. Vector plots of the associated normal modes are shown in Fig. 1. The cuts show that many interesting features are present in the excited states of benzene. The quality of the fitted model is seen by how closely the curves fit the points. The root-mean square deviation (RMSD) between the ab initio points and the model surfaces at the points is 0.055 eV over the 2436 datasets. An exponential weighting $w_i = \exp(E_i - E_0)$, where E_i is the ab initio energy at a point and E_0 is the energy of the relevant adiabatic surface at $\mathbf{Q}_0$, can be used to enhance the importance of low energy regions. When this is used, the RMSD drops to 0.0048 eV and thus most of the large errors lie in regions unlikely to be visited.

3.1. The parameters

Table 4 lists the on-diagonal linear coupling parameters, $\kappa_\alpha^{(i)}$. For all states these are non-zero for the two totally symmetric modes $\nu_1(1a_{1g})$ and $\nu_2(2a_{1g})$. The importance of a parameter is related to the ratio $\kappa_\alpha^{(i)}/\omega_\alpha$, the distance the minimum of the ground-state harmonic potential is shifted by the coupling. As the frequencies are 0.1292 and 0.4198 eV, respectively, the parameters for the lower frequency mode play a more important

Table 4
On-diagonal linear coupling constants, $\kappa_\alpha^{(i)}$, for the normal modes of benzene, ν_α, at the D_{6h} minimum energy geometry obtained by fitting the vibronic coupling model Hamiltonian to the adiabatic surfaces calculated at the SA-CAS(6,6)/6-31G* level

Mode	B_{2u}	B_{1u}	$E_{1u,x}$	$E_{1u,y}$	$E_{2g,x}$	$E_{2g,y}$
$\nu_1(1a_{1g})$	0.272	0.150	0.211	0.211	0.410	0.410
$\nu_2(2a_{1g})$	0.253	0.272	0.256	0.256	0.220	0.220
$\nu_{6a}(1e_{2g,x})$	–	–	−0.034	−0.034	−0.031	−0.031
$\nu_{7a}(4e_{2g,x})$	–	–	–	–	−0.031	0.031
$\nu_{8a}(3e_{2g,x})$	–	–	–	–	0.156	−0.156
$\nu_{9a}(2e_{2g,x})$	–	–	−0.018	0.018	−0.151	0.151

Electronic states are identified by their symmetry label. All values in eV.

Table 5
Off-diagonal linear coupling constants, $\lambda_\alpha^{(i,j)}$, for the normal modes of benzene, ν_α, at the D_{6h} minimum energy geometry obtained by fitting the vibronic coupling model Hamiltonian to the adiabatic surfaces calculated at the SA-CAS(6,6)/6-31G* level

	B_{2u}	B_{1u}	$E_{1u,x}$	$E_{1u,y}$	$E_{2g,x}$	$E_{2g,y}$
A_{1g}	$\nu_{14} = 0.295$ $\nu_{15} = 0.426$	–	–	–	$\nu_{8a} = 0.249$	$\nu_{8b} = 0.249$
B_{2u}		–	$\nu_{6b} = 0.018$	$\nu_{6a} = 0.018$	$\nu_{18b} = 0.153$ $\nu_{19b} = 0.122$	$\nu_{18a} = 0.153$ $\nu_{19a} = 0.122$
B_{1u}			$\nu_{6a} = 0.069$ $\nu_{8a} = -0.268$ $\nu_{9a} = 0.149$	$\nu_{6b} = 0.069$ $\nu_{8b} = -0.268$ $\nu_{9b} = 0.149$	$\nu_{18a} = 0.015$	$\nu_{18b} = 0.015$
$E_{1u,x}$				$\nu_{6b} = 0.034$ $\nu_{9b} = 0.018$	–	–
$E_{1u,y}$					–	–
$E_{2g,x}$						$\nu_{6b} = 0.031$ $\nu_{7b} = 0.031$ $\nu_{8b} = 0.156$ $\nu_{9b} = 0.151$

Electronic states are identified by their symmetry label. All values in eV.

role by a factor of 3 than parameters of the high frequency mode of similar strength. The parameters of the $\tilde{A}$ and $\tilde{D}$ states are especially strong along ν_1.

The $\tilde{C}$ and $\tilde{D}$ states are doubly degenerate and vibrational modes with e_{2g} symmetry also can have non-zero linear coupling parameters, that is they are Jahn–Teller active. There are four such pairs of modes $\nu_6(1e_{2g})$, $\nu_9(2e_{2g})$, $\nu_8(3e_{2g})$ and $\nu_7(4e_{2g})$. The x component goes to a_g symmetry at D_{2h} and so these modes appear on the diagonal of the model. Notice that the parameters have opposite signs for the two components of the state due to the symmetry of the Jahn–Teller interaction. As shown in Table 4 the coupling is in general weak. No value is listed for modes ν_8 and ν_7 for state $\tilde{C}$ as the couplings are insignificant ($\kappa_\alpha^{(i)}/\omega_\alpha < 0.05$). The strongest Jahn–Teller coupling is for the $\tilde{D}$ state along ν_9.

The linear off-diagonal coupling parameters are reported in Table 5. Non-zero parameters are possible for various modes for

Table 6
Components of the gradients, $\kappa_\alpha^{(i)}$, and the derivative coupling vectors, $\lambda_\alpha^{(i,j)}$, along the normal modes of benzene, ν_α at the ground-state D_{6h} minimum energy geometry

$\kappa_1^{(2)} = 0.2313$	$\kappa_2^{(2)} = -0.0543$	$\lambda_{15}^{(1,2)} = 0.5478$	$\lambda_{14}^{(1,2)} = 0.3536$
$\kappa_1^{(3)} = 0.1119$	$\kappa_2^{(3)} = -0.0374$		
$\kappa_1^{(4)} = 0.1712$	$\kappa_2^{(4)} = -0.0499$	$\lambda_{6b}^{(3,4)} = -0.0272$	
$\kappa_1^{(5)} = 0.1712$	$\kappa_2^{(5)} = -0.0499$		
$\kappa_1^{(6)} = 0.3694$	$\kappa_2^{(6)} = -0.0873$	$\lambda_{18b}^{(2,6)} = 0.5478$	$\lambda_{19b}^{(2,6)} = 0.3536$
$\kappa_1^{(7)} = 0.3664$	$\kappa_2^{(7)} = -0.0869$	$\lambda_{7b}^{(6,7)} = 0.0260$	$\lambda_{8b}^{(6,7)} = 0.2774$
		$\lambda_{9b}^{(6,7)} = 0.1533$	
$\kappa_{6a}^{(4)} = 0.0389$	$\kappa_{9a}^{(4)} = 0.0194$		
$\kappa_{8a}^{(4)} = 0.0432$			
$\kappa_{6a}^{(5)} = -0.0389$	$\kappa_{9a}^{(5)} = -0.0194$	$\lambda_{6b}^{(4,5)} = -0.0389$	$\lambda_{9b}^{(4,5)} = 0.0194$
$\kappa_{8a}^{(5)} = -0.0432$		$\lambda_{8b}^{(4,5)} = 0.0432$	
$\kappa_{6a}^{(6)} = 0.0179$	$\kappa_{9a}^{(6)} = -0.1527$		
$\kappa_{8a}^{(6)} = -0.2826$	$\kappa_{7a}^{(6)} = 0.0306$		
$\kappa_{6a}^{(7)} = -0.0228$	$\kappa_{9a}^{(7)} = 0.1627$	$\lambda_{6b}^{(6,7)} = 0.0179$	$\lambda_{9b}^{(6,7)} = 0.1527$
$\kappa_{8a}^{(7)} = 0.3008$	$\kappa_{7a}^{(7)} = -0.0320$	$\lambda_{8b}^{(6,7)} = 0.2826$	$\lambda_{7b}^{(6,7)} = 0.0306$

Superscripts relate to the electronic states. Values in eV, calculated at the CASSCF(6,6)/6-31G* level.

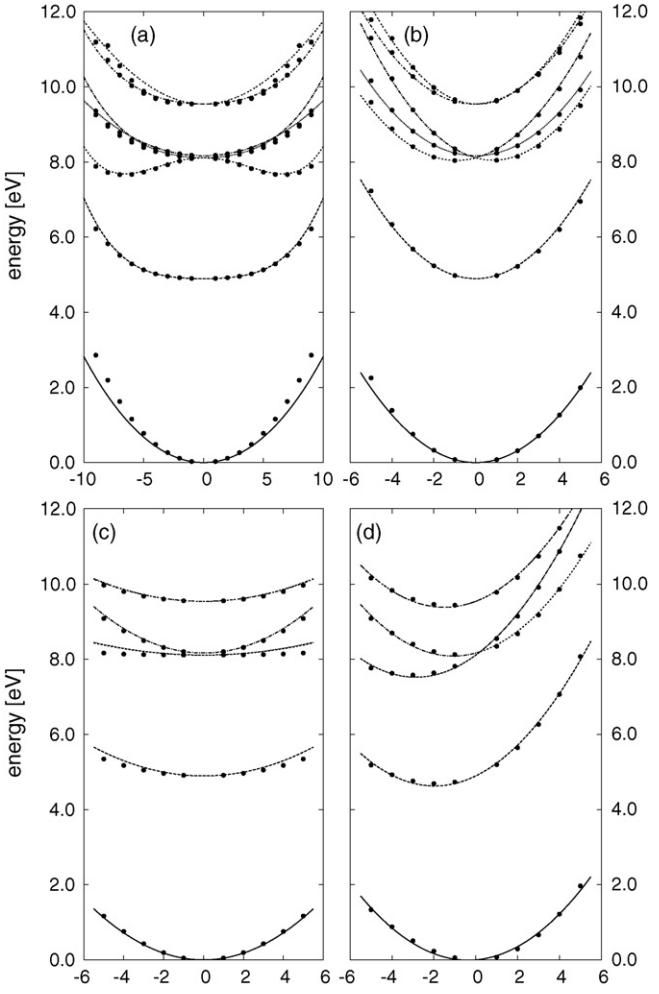

Fig. 2. Cuts through the adiabatic potential energy surfaces of benzene for the ground-state and lowest six excited states. In order of energy these are: $\tilde{X}^1A_{1g}$, $\tilde{A}^1B_{2u}$, $\tilde{D}^1E_{2g}$, $\tilde{B}^1B_{1u}$, and $\tilde{C}^1E_{1u}$. The points are results from ab initio calculations at the CAS(6,6)//6-31G* level, and the lines are from the model Hamiltonian fitted to the points: (a) $\nu_{16a}(1e_{2u})$, the boat mode; (b) $\nu_{6a}(1e_{2g})$, a quinoid mode; (c) $\nu_4(1b_{2g})$, the chair mode; (d) $\nu_1(1a_{1g})$, the carbon breathing mode.

Table 7
On-diagonal quadratic coupling constants, $\gamma^{(i)}_{\alpha\alpha}$ for the normal modes, ν_α, of benzene at the D_{6h} minimum energy geometry obtained by fitting the vibronic coupling model Hamiltonian to the adiabatic surfaces calculated at the SA-CAS(6,6)/6-31G* level

Mode	B_{2u}	B_{1u}	$E_{1u,x}$	$E_{1u,y}$	$E_{2g,x}$	$E_{2g,y}$
ν_1	–	0.011	0.011	0.011	0.014	0.014
ν_2	0.040	0.043	0.043	0.043	0.040	0.040
ν_4	−0.039	–	−0.050	−0.051	−0.069	−0.068
ν_5	−0.034	–	−0.024	−0.024	−0.071	−0.071
ν_{6a}	−0.014	−0.011	–	–	−0.015	–
ν_{6b}	−0.014	−0.011	–	–	−0.015	–
ν_7	0.062	0.065	0.065	0.067	0.061	0.063
ν_8	0.020	0.019	0.023	0.019	0.023	−0.011
ν_9	0.016	0.016	0.017	0.015	0.023	–
ν_{10a}	−0.042	0.014	0.036	0.034	−0.063	−0.084
ν_{10b}	−0.042	−0.014	−0.034	−0.036	−0.084	−0.063
ν_{11}	−0.013	–	–	–	−0.026	−0.026
ν_{12}	–	–	–	–	−0.014	−0.014
ν_{13}	0.040	0.044	0.044	0.043	0.040	0.040
ν_{14}	0.054	0.069	0.050	0.050	0.053	0.075
ν_{15}	0.114	0.147	0.097	0.097	0.153	0.099
ν_{16a}	−0.042	−0.026	−0.031	–	−0.093	−0.030
ν_{16b}	−0.042	−0.026	–	−0.031	−0.030	−0.093
ν_{17a}	−0.053	–	−0.045	−0.025	−0.131	−0.062
ν_{17b}	−0.053	–	−0.025	−0.045	−0.062	−0.131
ν_{20}	0.061	0.063	0.063	0.063	0.062	0.063

Electronic states are identified by their symmetry label. All values in eV.

pairs of states dependent on the symmetries as listed in Table 3. Only significant parameters, with a value of $\lambda_\alpha/\omega_\alpha > 0.05$ are listed in the upper half of the matrix of pairs of states. Three types of coupling can be identified.

The Jahn–Teller coupling involves the y component of the e_{2g} modes, i.e. the complement to the component discussed above with respect to the on-diagonal parameters. The values are identical to the on-diagonal parameters as shown in Eq. (14).

Between the singly degenerate state $\tilde{X}$, $\tilde{A}$ and $\tilde{B}$, simple vibronic coupling occurs. Strong coupling is found between $\tilde{X}$ and $\tilde{A}$ along the $\nu_{15}(1b_{2u})$ and $\nu_{14}(2b_{2u})$. The large energy gap between the states means that this does not lead to a conical intersection between the states, but introduces anharmonicity into the surfaces. There is no significant coupling between the $\tilde{B}$ state with either $\tilde{X}$ or $\tilde{A}$. The former could happen along $\nu_{12}(1b_{1u})$ and $\nu_{13}(2b_{1u})$ and the latter through $\nu_3(1a_{2g})$ but these parameters are all negligible.

The pseudo-Jahn–Teller couplings form the final set. These couple a singly degenerate state with a doubly degenerate one along a doubly degenerate vibrational mode: each component of the mode couples to a different component of the doubly degenerate state and the degeneracy is split in a similar, if topologically

Table 8
On-diagonal quartic coupling constants, $\epsilon^{(i)}_\alpha$ for the normal modes of benzene, ν_α, at the D_{6h} minimum energy geometry obtained by fitting the vibronic coupling model Hamiltonian to the adiabatic surfaces calculated at the SA-CAS(6,6)/6-31G* level

Mode	A_{1g}	B_{2u}	B_{1u}	$E_{1u,x}$	$E_{1u,y}$	$E_{2g,x}$	$E_{2g,y}$
ν_{10a}	0.0205	0.0222	0.0202	0.0216	0.0225	0.0223	0.0260
ν_{10b}	0.0205	0.0222	0.0202	0.0225	0.0216	0.0260	0.0223
ν_{11}	0.0250	0.0210	0.0235	0.0221	0.0221	0.0187	0.0187
ν_{15}	0.0660	–	–	–	–	–	–
ν_{16a}	–	0.0038	–	0.0020	–	0.0054	0.0023
ν_{16b}	–	0.0038	–	–	0.0020	0.0023	0.0054
ν_{17a}	0.0142	0.0179	0.0131	0.0197	0.0176	0.0254	0.0165
ν_{17b}	0.0142	0.0179	0.0131	0.0176	0.0197	0.0165	0.0254

Electronic states are identified by their symmetry label. All values in eV.

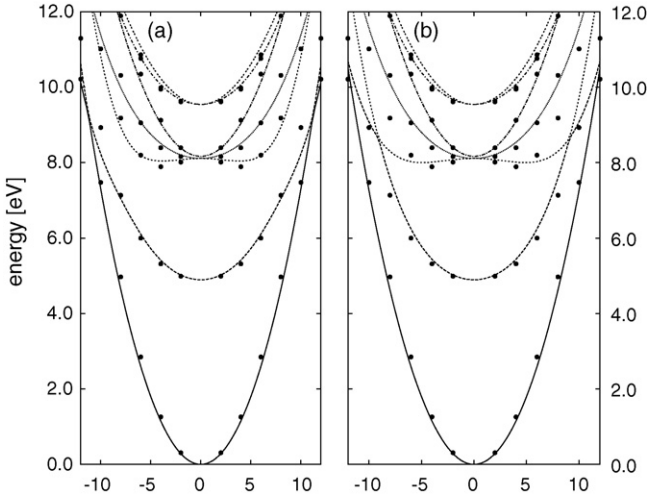

Fig. 3. Cuts through the adiabatic potential energy surfaces of benzene for the ground-state and lowest six excited states. In order of energy these are: $\tilde{X}^1A_{1g}$, $\tilde{A}^1B_{2u}$, $\tilde{D}^1E_{2g}$, $\tilde{B}^1B_{1u}$, and $\tilde{C}^1E_{1u}$. The points are results from ab initio calculations at the CAS(6,6)//6-31G* level, and the lines are from the model Hamiltonian fitted to the points. Both plots are along a diagonal between $\nu_{16a}(1e_{2u})$ the boat mode and $\nu_4(1b_{2g})$ the chair mode: (a) including the second-order pseudo-Jahn–Teller coupling between $\tilde{B}$ and $\tilde{D}$; (b) without the second-order pseudo-Jahn–Teller coupling.

different way to normal Jahn–Teller coupling. In benzene, the $\tilde{X}^1A_{1g}$ state couples the $\tilde{C}^1E_{1u}$ state via the e_{1u} modes and the $\tilde{D}^1E_{2g}$ state via the e_{2g} modes. Only $\tilde{X}$–$\tilde{D}$ coupling along the ν_8 modes is non-negligible, with $\nu_{8a}(3e_{2g,x})$ coupling to $\tilde{D}^1E_{2g,x}$ and $\nu_{8b}(3e_{2g,y})$ coupling to $\tilde{D}^1E_{2g,y}$.

The $\tilde{A}^1B_{2u}$ and $\tilde{B}^1B_{1u}$ states both couple to the $\tilde{C}^1E_{1u}$ state along the e_{2g} modes, with the components coupling as shown in Table 5. Some of these parameters are very significant, particularly between the neighbouring $\tilde{B}$ and $\tilde{C}$ states. They would, however, not be easy to distinguish from the Jahn–Teller coupling in the $\tilde{C}$ state if only the adiabatic surfaces are examined. In fact the $\tilde{B}$–$\tilde{C}$ pseudo-Jahn–Teller coupling dominates the lifting of the degeneracy along modes ν_8 and ν_9, while it is of comparable importance to the Jahn–Teller coupling along ν_6. The $\tilde{A}$ and $\tilde{B}$ states also couple to the $\tilde{D}^1E_{2g}$ state using pseudo-Jahn–Teller coupling along the e_{1u} modes. In contrast to the coupling to the $\tilde{C}$ state, this is the only coupling that splits the degeneracy along these modes, and is especially strong for the $\tilde{B}$–$\tilde{D}$ coupling along the $\nu_{18}(1e_{1u})$ modes.

In many cases, the linear coupling forms the major part of the non-adiabatic coupling, and will alone describe the features of the potential energy surfaces. This is also the case for benzene, with the exception of the lowest frequency mode $\nu_{16}(1e_{2u})$. In fact, excluding this doubly degenerate mode the model Hamiltonian with linear coupling alone has an RMSD of 0.134 eV on the calculated points.

The linear coupling constants should be similar to the elements of the potential gradients and non-adiabatic coupling vectors which can be calculated directly using the Gaussian03 program. The latter can, however, only be obtained for neighbouring states. They will not be identical as the vectors are a local property calculated at $\mathbf{Q}_0$, while the fitting procedure means that the coupling constants take into account the form of the potential surfaces away from the Franck–Condon point. The vector components along the dimensionless normal modes are listed in Table 6. Note that values of the non-adiabatic coupling are for neighbouring states in the quantum chemistry calculations rather the correct ordering of states. The values are indeed seen to be similar in magnitude and sign to the model parameters in Tables 4 and 5. The exception is the high frequency ν_2 mode which has much larger parameters in the fitted model. This is due to the significant anharmonicity of the mode which is not well accounted for in the harmonic model.

The frequencies of the excited states are changed from the ground-state values by the on-diagonal second-order parameters $\gamma^{(i)}_{\alpha\alpha}$. By definition values for the ground-state $\gamma^{(1)}_{\alpha\alpha}$ are zero. Due to the coordinate scaling used in the Hamiltonian, the frequency of a mode with potential:

$$V = \tfrac{1}{2}(\omega_\alpha + \gamma^{(i)}_{\alpha\alpha})Q^2_\alpha$$

is $\sqrt{\omega^2_\alpha + \omega_\alpha\gamma^{(i)}_{\alpha\alpha}}$. Thus a 5% change in the frequency is given by a ratio:

$$\left|\frac{\gamma^{(i)}_{\alpha\alpha}}{\omega_\alpha}\right| > 0.1$$

Significant values (a ratio over 0.05) are listed in Table 7. Negative values correspond to a lowering of frequency.

In general the on-diagonal quadratic parameters are a small effect, with a ratio of around 0.1. A noticeable effect is found along the chair-mode, ν_4, with a significant lowering of frequency except in the $\tilde{B}$ state. A significant increase in frequency is also found for all states along the b_{2u} modes ν_{14} and ν_{15}. Of particular interest here are modes ν_{10}, ν_{16} and ν_{17}. These are all doubly degenerate modes with large quadratic couplings. Furthermore the different components couple differently with the two components of the doubly degenerate electronic states. Scaling the coordinates to an appropriate new frequency the second-order coupling matrix for these modes and a pair of states can be written

$$W^{(2)}_{\{i,i+1\}} = \begin{pmatrix} \gamma^{(i)}_{\alpha\alpha}(Q^2_{\alpha,x} - Q^2_{\alpha,y}) & \mu^{(i,i+1)}_{\alpha\alpha}Q_{\alpha,x}Q_{\alpha,y} \\ \mu^{(i,i+1)}_{\alpha\alpha}Q_{\alpha,x}Q_{\alpha,y} & \gamma^{(i+1)}_{\alpha\alpha}(Q^2_{\alpha,x} - Q^2_{\alpha,y}) \end{pmatrix},$$
$$\gamma^{(i)}_{\alpha\alpha} = -\gamma^{(i+1)}_{\alpha\alpha} = \mu^{(i,i+1)}_{\alpha\alpha} \quad (17)$$

Note the symmetry constraint on the constants analogous to that on the linear Jahn–Teller constants in Eq. (14). This second-order Jahn–Teller coupling leads to the formation of three minima on the lower adiabatic surface of the coupled pair [21].

Bilinear constants, $\gamma^{(i)}_{\alpha\beta}, \alpha \neq \beta$ are usually small if the quadratic constants of the modes are small, and with the exception of the second-order Jahn–Teller constants just described these have not been calculated. With one exception, second-order off-diagonal coupling constants have also not been calculated as they also are usually small. The exception is the coupling along a diagonal between ν_{16} and ν_4. These modes are the boat/twist and chair modes and have e_{2u} and b_{2g} symmetry, respectively. Thus the coupling constant $\mu^{(2,6)}_{4,16}$ is non-zero as the product of symmetries of the two modes is e_{1u} which according to Table 3 can couple states $\tilde{A}$ and $\tilde{D}$. A value of

$$\mu^{(2,6)}_{4,16} = 0.0129\,\text{eV} \quad (18)$$

was found by the fit, and as will be shown below this is a crucial parameter for the surfaces around the S_1/S_0 conical intersection.

The final parameters in the model are the on-diagonal quartic parameters that were added along selected modes. The selection was made purely by inspection of the quadratic fit. The modes were ν_{10}, ν_{11}, ν_{15}, ν_{16} and ν_{17} and the parameters are listed in Table 8. With the exception of ν_{11} these modes all have large quadratic constants. In cases where the ground-state value is the same as the excited state values, the effect is due to a general anharmonicity along the mode at large value.

3.2. Cuts through the potential energy surfaces

Along the breathing mode, ν_1, (Fig. 2(d)) the upper states are shifted relative to the ground-state, as expected for a totally symmetric mode due to the non-zero on-diagonal linear coupling. This shift is especially strong for the $\tilde{A}$ and $\tilde{D}$ states, which also seem to have a significant change in frequency from

the ground-state. Along the boat mode, ν_4, the non-totally symmetric symmetry means that there is no shift of equilibrium geometry, but there is a significant change of frequency in the $\tilde{A}$, $\tilde{D}$ and $\tilde{C}$ states (Fig 2(c)). This is particularly noticeable for the $\tilde{D}$ state, which is nearly flat along this mode.

The quinoid modes, ν_6, are a doubly degenerate pair with e_{2g} symmetry. They are thus Jahn–Teller active for the two doubly degenerate states $\tilde{C}$ and $\tilde{D}$. This is seen by the splitting of these states in Fig. 2(b). The splitting of the $\tilde{C}$ state is very small. Only the cut along ν_{6a} is shown: along ν_{6b} the surfaces look identical. The $\tilde{B}$ state surface runs through the middle of the split $\tilde{D}$ pair, but there is no coupling between these states along this mode.

Of particular interest is the behaviour along the boat/twist modes ν_{16}, of which the cut along ν_{16a} is shown in Fig. 2(a). The cut along ν_{16b} looks identical. These are the lowest frequency modes with an experimental frequency of only 430 cm^{-1}. The symmetry is e_{2u} so all the linear coupling parameters are zero. Despite this, the degenerate states $\tilde{C}$ and $\tilde{D}$ are split, the latter very strongly, along these modes. This is thus due to second-order Jahn–Teller coupling, i.e. the coupling between the states is due to quadratic terms. It is also clear that the $\tilde{A}$ surface is not harmonic. This is not due to coupling with any other surfaces, but is simply significant changes to the bonding on excitation lead to significant quadratic and quartic terms for this state along this mode.

Motion along a direction diagonally between ν_{16a} and ν_6 corresponds to a combination of boat and chair that is effectively one corner of the molecule lifting out of the plane (Fig. 1(e)). This motion thus leads to prefulvene. The cut along this combination mode is shown in Fig. 3(a) and the surfaces for the $\tilde{X}$ and $\tilde{A}$ states are seen to intersect around $Q_{16a} = Q_6 = \pm 10$. This is part of the S_0/S_1 conical intersection seam found to lead to prefulvene by Palmer et al. [2].

In the previous section it was mentioned that a significant bilinear coupling (a second-order pseudo-Jahn–Teller coupling) was found along this direction between the $\tilde{A}$ and $\tilde{D}$ states. The effect of this term is seen by the difference between Fig. 3(a) and (b)—the coupling is included in the former and not in the latter. The difference is staggering given the small parameter. Ignoring $\mu^{(2,6)}_{4,16}$ leads to a completely different interpretation of the intersection. The crossing is now at higher energy and the S_0/S_1 conical intersection is between the $\tilde{X}$ and $\tilde{D}$ states. The $\tilde{A}$ and $\tilde{D}$ states also now cross. Adding the coupling parameter between these states the surfaces for the $\tilde{A}$ and $\tilde{D}$ states do not cross and the fit is better. This coupling could also lead to a barrier being formed near the conical intersection due to an avoided crossing between the $\tilde{A}$ and $\tilde{D}$ states.

4. Discussion and conclusion

The dynamic behaviour of a molecule can be rationalised by the topology of its potential energy surfaces. For a system in which vibronic coupling is important, the diabatic surfaces and the coupling between them forms the appropriate reference: the diabatic states can be related to an electronic configuration, a "chemical species", and the coupling allows transitions to occur between them. The diabatic surfaces are in general smoother than the adiabatic ones, which are the eigenvalues of the electronic Hamiltonian, the usual "potential energy surfaces". The vibronic coupling model embodies this, providing the diabatic surfaces using smooth functions, and finding the couplings by fitting to adiabatic surfaces. Benzene represents an ambitious target with seven coupled states and 30 vibrational modes, but the automatic fitting procedure used here is able to provide the necessary parameters.

Due to the linear optimisation used there is unfortunately no guarantee that the parameters obtained are the best, and it is possible that a different set of parameters would obtain a similar, or even better, fit. The procedure used, taking a good initial guess and first optimising the more important linear parameters before adding the higher order terms, aims to get around these problems in a rather manual way. Better analysis of the result, e.g. an idea of the sensitivity of the fit to the parameters, is needed. Despite this, and despite the simplicity of the model, the model surfaces obtained fit those obtained from quantum chemistry calculations very well. As a results we are able to perform a full vibronic coupling analysis of the features of the surfaces.

Vibronic couplings are conveniently characterised according to the symmetry of the states and modes involved, and the power of the coordinate with which the leading term is found. In benzene many types are present. Jahn–Teller interaction is found in the E_{2g} and E_{1u} states via the e_{2g} modes. The same modes couple the doubly degenerate E_{1u} states to the singly degenerate B_{2u} and B_{1u} states using pseudo-Jahn–Teller interactions, while e_{1u} modes couple the E_{2g} to the B_{1u} and B_{2u} states. It was found that there is particularly strong second-order Jahn–Teller coupling that splits the doubly degenerate states along the low-frequency e_{2u} boat/twist mode.

Also significant is the strong second-order pseudo-Jahn–Teller coupling that is found between the $\tilde{A}^1B_{2u}$ and $\tilde{D}^1E_{2g}$ states. This coupling repulses the two surfaces and allows the S_0/S_1 conical intersection to form between the $\tilde{X}^1A_{1g}$ and $\tilde{A}^1B_{2u}$ states as prefulvene is approached along the diagonal of Q_{16}, Q_4. The surfaces are thus consistent with the known photophysics of benzene for the $\tilde{A}$ state, excepting the absolute value of energies which are too high due to the lack of dynamic correlation in the quantum chemistry calculations.

What cannot be easily explained by the model is the photophysics of the $\tilde{B}$ state that is known to decay rapidly to the ground-state without appreciably populating the $\tilde{A}$ state. This leads to the expectation of a non-adiabatic pathway connecting the two states directly, which is not found. In fact the present model shows only a minimal coupling between the $\tilde{B}$ and the lower $\tilde{X}$ or $\tilde{A}$ states. This is most likely due to the poor description of the $\tilde{B}$ state by the CASSCF method used, which is underestimating the coupling. The vibronic coupling analysis, however, means that we know where to look, i.e. which modes must be involved in the missing coupling.

The model detailed here can now be refined using higher level calculations and experimental information. This will result in an analytic representation suitable for the calculation of the absorption spectrum and photophysical processes that are dominated by the dynamics close to the Franck–Condon point. More

work, however, will be needed to provide surfaces suitable for the photochemistry of benzene. For this we will need to examine the regions around the conical intersections in more detail and add this information so that the surfaces also provide a good description of the photoproducts.

Acknowledgements

Thanks are due to Benjamin Lasorne, Mike Bearpark and Mike Robb for help on using the CAS method and to Helen Fielding for discussions on the photochemistry of benzene. This work is part of a project to control the photochemistry of benzene funded by the EPSRC GR/T20311/01.

References

[1] A. Toniolo, A.L. Thompson, T. Martínez, Chem. Phys. 304 (2004) 133–145.
[2] I.J. Palmer, I.N. Ragazos, F. Bernardi, M. Olivucci, M.A. Robb, J. Am. Chem. Soc. 115 (1993) 672–682.
[3] B.O. Roos, K. Andersson, M.P. Fülscher, Chem. Phys. Lett. 192 (1992) 5–13.
[4] A. Bernhardsson, N. Forsberg, P.-Å. Malmqvist, B.O. Roos, J. Chem. Phys. 112 (2000) 2798–2809.
[5] O. Christiansen, J.F. Stanton, J. Gauss, J. Chem. Phys. 108 (1998) 3987–4001.
[6] L. Lorentzon, P.-Å. Malmqvist, M. Fülscher, B.O. Roos, Theor. Chim. Acta 91 (1995) 91–108.
[7] L.T. Scott, M. Jones Jr., Chem. Rev. 72 (1972) 181–202.
[8] D. Bryce-Smith, A. Gilbert, Tetrahedron 32 (1972) 1309–1326.
[9] J. Philis, A. Bolovinos, G. Andritsopoulos, E. Pantos, P. Tsekeris, J. Phys. B 14 (1981) 3621–3635.
[10] C.S. Parmenter, Adv. Chem. Phys. 22 (1972) 365–421.
[11] M. Clara, T. Hellerer, H.J. Neusser, Appl. Phys. B 71 (2000) 431.
[12] E.N. Lassetre, A. Skerbele, M.A. Dillon, K.J. Ross, J. Chem. Phys. 48 (1968) 5066.
[13] N. Nakashima, H. Inoue, M. Sumitania, K. Yoshihara, J. Chem. Phys. 73 (1980) 5976.
[14] K.C. Kulander (Ed.), Time-dependent Methods for Quantum Dynamics, Elsevier, Amsterdam, 1991.
[15] R.E. Wyatt, J.Z.H. Zhang (Eds.), Dynamics of Molecules and Chemical Reactions, Marcel Dekker, New York, 1996.
[16] R. Kosloff, J. Phys. Chem. 92 (1988) 2087–2100.
[17] M.H. Beck, A. Jäckle, G.A. Worth, H.-D. Meyer, Phys. Rep. 324 (2000) 1–105.
[18] M. Klessinger, Angew. Chem. 107 (1995) 597.
[19] M.A. Robb, F. Bernardi, M. Olivucci, Pure Appl. Chem. 67 (1995) 783–789.
[20] W. Domcke, D.R. Yarkony, H. Köppel (Eds.), Conical Intersections: Electronic Structure, Dynamics and Spectroscopy, World Scientific, Singapore, 2004.
[21] G.A. Worth, L.S. Cederbaum, Ann. Rev. Phys. Chem. 55 (2004) 127–158.
[22] M.A. Robb, M. Garavelli, M. Olivucci, F. Bernardi, A computational strategy for organic photochemistry, in: Reviews in Computational Chemistry, vol. 15, John Wiley and Sons, New York, 2000, pp. 87–146.
[23] W. Radloff, T. Freudenberg, H.-H. Ritze, V. Stert, K. Weyers, F. Noack, Chem. Phys. Lett. 245 (1995) 400.
[24] H. Köppel, W. Domcke, L.S. Cederbaum, Adv. Chem. Phys. 57 (1984) 59–246.
[25] H. Köppel, M. Döscher, I. Baldea, H.-D. Meyer, P.G. Szalay, J. Chem. Phys. 117 (2002) 2657–2671.
[26] H.-D. Meyer, U. Manthe, L.S. Cederbaum, Chem. Phys. Lett. 165 (1990) 73–78.
[27] G. Worth, H.-D. Meyer, L. Cederbaum, Multidimensional dynamics involving a conical intersection: wavepacket calculations using the MCTDH method, in: Conical Intersections: Electronic Structure, Dynamics and Spectroscopy, World Scientific, Singapore, 2004, pp. 583–617.
[28] A. Markmann, G.A. Worth, L.S. Cederbaum, J. Chem. Phys. 122 (2005) 144315–144320.
[29] G.A. Worth, M.H. Beck, A.Jäckle, H.-D. Meyer, The MCTDH Package, Version 8.3, see http://www.pci.uni-heidelberg.de/tc/usr/mctdh/, 2003.
[30] C. Cattarius, G.A. Worth, H.-D. Meyer, L.S. Cederbaum, J. Chem. Phys. (2001) 2088–2100.
[31] G.A. Worth, G. Welch, M.J. Paterson, Mol. Phys. 104 (2006) 1095–1105.
[32] M.J. Frisch, G.W. Trucks, H.B. Schlegel, G.E. Scuseria, M.A. Robb, J.R. Cheeseman, J.A. Montgomery, T. Vreven, K.N. Kudin, J.C. Burant, J.M. Millam, S.S. Iyengar, J. Tomasi, V. Barone, B. Mennucci, M. Cossi, G. Scalmani, N. Rega, G.A. Petersson, H. Nakatsuji, M. Hada, M. Ehara, K. Toyota, R. Fukuda, J. Hasegawa, M. Ishida, T. Nakajima, Y. Honda, O. Kitao, H. Nakai, M. Klene, X. Li, J.E. Knox, H.P. Hratchian, J.B. Cross, V. Bakken, C. Adamo, J. Jaramillo, R. Gomperts, R.E. Stratmann, O. Yazyev, A.J. Austin, R. Cammi, C. Pomelli, J.W. Ochterski, P.Y. Ayala, K. Morokuma, G.A. Voth, P. Salvador, J.J. Dannenberg, V.G. Zakrzewski, S. Dapprich, A.D. Daniels, M.C. Strain, O. Farkas, D.K. Malick, A.D. Rabuck, K. Raghavachari, J.B. Foresman, J.V. Ortiz, Q. Cui, A.G. Baboul, S. Clifford, J. Cioslowski, B.B. Stefanov, G. Liu, A. Liashenko, P. Piskorz, I. Komaromi, R.L. Martin, D.J. Fox, T. Keith, M.A. Al-Laham, C.Y. Peng, A. Nanayakkara, M. Challacombe, P.M.W. Gill, B. Johnson, W. Chen, M.W. Wong, C. Gonzalez, J.A. Pople Jr., Gaussian 03, Revision C.02, Gaussian, Inc., Pittsburgh, PA, 2003.
[33] E.B. Wilson Jr., Phys. Rev. 45 (1934) 706.
[34] G. Herzberg, Infrared and Raman Spectroscopy, Van Nostrand, Princeton, NJ, USA, 1945, p. 118.
[35] L. Goodman, A.G. Ozkabak, A.N. Thakur, J. Phys. Chem. 95 (1991) 9044–9058.